Chapter 5

Analysis of multiple parallel cracks in a functionally graded magneto-electro-elastic plane using boundary collocation method

5.1 Introduction

Intelligent materials made of piezoelectric and piezomagnetic materials have been widely used in medical ultrasonic imaging, chips of magnetic sensors, magnetic-field probes, acoustic, hydrophones, sensors, electric packaging, and actuators in the smart structures and components of energy harvesters [81]. The coupled properties of piezoelectric and piezomagnetic composites offer the scope to engineers to create intelligent structures, composite materials, and devices those are capable of responding to internal and/or environmental changes. One such composite material is magneto-electro-elastic material having the combined effects of piezoelectric, piezomagnetic, and magneto-electric. Magneto-electro-elastic materials are used in

electronic instrumentations and microwave and optoelectronics. Nowadays, the use of functionally graded materials (FGMs) in the engineering field is unavoidable due to their capability of reducing the concentration of stress and increasing fracture toughness.

Eventually, the concept of FGMs is extended to magneto-electro-elastic materials to enhance the reliability of composites. These materials have continuously varying properties which are considered as functionally graded magneto-electro-elastic (FGMEE) materials. These materials have the advantage that they have neither internal seams nor desirable boundaries. However owing to the brittleness, cracks inevitably exist in FGMEE materials. For such types of materials having cracks subjected to magneto-electro-mechanical loadings, the magneto-electro-elastic field is concentrated near cracks, which causes the advancement of cracks and as a result, the degradation of the performance of magneto-electro-elastic materials found to occur. Also during the manufacturing process, unavoidable initiations of cracks, holes, inclusions, dislocation, and other defects occur. These defects cause premature failure of composites or structures at any moment that finally leads to failure. Therefore, it is very much important to study the fracture behavior of FGMEE materials.

An anti-plane problem for an embedded and edge crack in a functionally graded magneto-electro-elastic strip is studied in [71] by using the integral transform and dislocation density functions. A similar problem for an embedded crack in a functionally graded piezoelectric/piezomagnetic plate was investigated in [13] using the boundary collocation method. In [21], an anti-plane internal crack normal to the edge of a functionally graded piezoelectric/piezomagnetic half-plane was considered in which the theory of energy density is applied to know the fracture behavior. A discussion on the kinking phenomena of impermeable and permeable moving cracks

in an FGMEE strip under anti-plane mechanical loading and in-plane electric and also magnetic loadings was presented in [40].

Since FGMEE materials are brittle in nature, they can usually contain multiple cracks with an extremely high crack density. The interaction between these cracks may significantly affect their fracture behavior. However less number of articles are available in the literature on such multi-crack problems in composites made of piezoelectric and piezomagnetic materials, and only a few studies are conducted [6, 43, 120**?**]. Moreover, due to the vulnerability, edge cracks are more catastrophic in comparison to embedded cracks. The problem of periodic surface cracks under thermal loading in a functionally graded composite was studied in [39, 60].

In general, the finite element method is used to calculate the crack tip SIF for cracked structures [78, 86]. However, due to various difficulties including the determination of a large number of unknowns, and consideration of a large number of node points, this method is sometimes complex to calculate crack tip SIF. To overcome this, the method of the integral equation and others [102, 103, 104, 105] are used. One of them is the boundary collocation method (BCM). In BCM the exact solutions of governing partial differential equations are used and approximations are restricted only to the boundaries. For approximation, the discretization of boundaries is accomplished. For BCM it is not required to discretize the domain of the problem and therefore the method is applied to problems with arbitrary boundary conditions and irregular domains. Therefore, BCM is an advantageous method to study crack problems due to its simplicity, accuracy, and less computational time. Muskhelishvili [80] has formulated some basic equations for solving the elasticity problem by using the complex variable function. An initiative has been taken by Williams [116] and Isida [56] in their works during solutions of the finite cracked

plane problems. If the crack surface is subjected to some loading in a finite cracked plane, then the complex potentials must satisfy the following conditions [74]:

1. The equilibrium and compatibility conditions in the occupied region of the crack plane.
2. Stress condition on the crack surface.
3. For multiply connected cracked plane, the single-valued condition of displacement around the crack.
4. The boundary conditions.

In most cases, the first three conditions are automatically satisfied. Only the boundary conditions need to be checked. Along with that for better accuracy, the least square method is used. The least-square technique is used to minimize the resultant force and also the displacement residuals along the boundary [85].

In light of the above discussion, the authors of the current chapter have concentrated on the issue of multiple parallel cracks in a finite FGMEE plane. According to [13, 40, 71], the material properties are assumed to vary exponentially along the x-axis. Both magneto-electrically impermeable and magneto-electrically permeable crack surface conditions are adopted in this study. Additionally, three distinct crack configuration cases are taken into account. In the first case, multiple parallel embedded cracks of the same length are considered, in the second, multiple parallel edge cracks of the same length are considered, and in the third, multiple parallel edge cracks of alternating lengths are taken into consideration. The problem is then reduced to power series form as per the considered case which is subsequently solved numerically with the aid of BCM and the least square approach. The semi-analytical forms of crack tip SIFs are obtained that help to determine the

expressions of crack tip SMFs. The outcome of the current study is also supported by an existing result for a specific case. The shielding and amplification phenomena of cracks can be identified using the semi-analytical forms of SMFs, which can be used to determine the likelihood of crack arrest. Through visual presentations for the three different crack configurations under consideration, an effort has been made to illustrate the effects of the gradient parameter, the distance between the cracks, and the electric and magnetic loadings on SMFs.

5.2 Mathematical formulation of the problem

5.2.1 Schematic description

Consider a finite number $(2N+1)$ of parallel cracks having length $b_m - a_m$ $(m = 0, \pm 1, ..., \pm N)$ in a finite magneto-electro-elastic plane of width w and height $2h$ as shown in Fig. 5.2.1a. Any two parallel cracks are separated by a distance of h_0. The magneto-electro-elastic plane exhibits transversely isotropic behaviour and is poled in the $z-$direction. The surfaces of the cracks are subjected to anti-plane mechanical τ_0, in-plane electric D_0, and magnetic B_0 loadings, as shown in Fig. 5.2.1b. Therefore, this article addresses the problem of an anti-plane elastic field coupled with in-plane electric and magnetic fields and the model is based on the framework of magneto-electrostatics.

The mechanical displacement, electric and magnetic potentials are denoted by w_m, ϕ_m, and ψ_m, respectively. c_{44}, e_{15}, f_{15}, ϵ_{11}, g_{11}, μ_{11} are the material constants viz., shear modulus, magnetic permeability, dielectric, piezoelectric, piezomagnetic

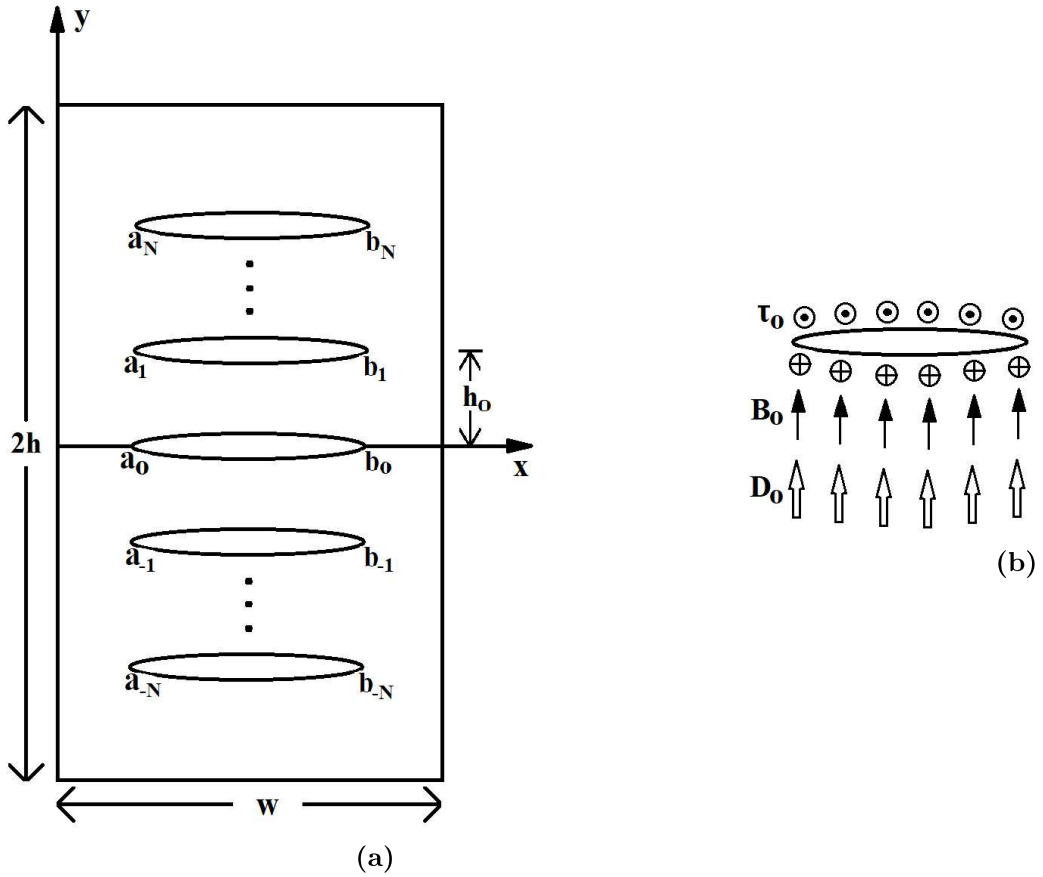

Figure 5.2.1: Schematic diagram of the problem.

and magneto-electric constants, respectively and expressed as

$$c_{44}(x) = c_{440}e^{\beta x},\ e_{15}(x) = e_{150}e^{\beta x},\ f_{15}(x) = f_{150}e^{\beta x}, \tag{5.2.1}$$

$$\epsilon_{11}(x) = \epsilon_{110}e^{\beta x},\ g_{11}(x) = g_{110}e^{\beta x},\ \mu_{11}(x) = \mu_{110}e^{\beta x}, \tag{5.2.2}$$

where β is the functionally graded parameter and c_{440}, μ_{110}, ϵ_{110}, e_{150}, f_{150}, g_{110} represent the material constants at $x = 0$. Throughout the chapter $m = 0, \pm 1, ..., \pm N$ denote the $2N + 1$ number of parallel edge cracks.

5.2.2 Governing equations and boundary conditions

The constitutive equations for infinitely small deformations are given by

$$\tau_{mzk} = c_{44}\frac{\partial w_m}{\partial k} + e_{15}\frac{\partial \phi_m}{\partial k} + f_{15}\frac{\partial \psi_m}{\partial k}, \tag{5.2.3}$$

$$D_{mk} = e_{15}\frac{\partial w_m}{\partial k} - \epsilon_{11}\frac{\partial \phi_m}{\partial k} - g_{11}\frac{\partial \psi_m}{\partial k}, \tag{5.2.4}$$

$$B_{mk} = f_{15}\frac{\partial w_m}{\partial k} - g_{11}\frac{\partial \phi_m}{\partial k} - \mu_{11}\frac{\partial \psi_m}{\partial k}, \tag{5.2.5}$$

where τ_{mzk}, D_{mk}, B_{mk} $(k = x, y)$ are the anti-plane shear stress, in-plane electric displacement, and magnetic inductions, respectively.

The equilibrium equations of the FGMEE plane for $m = 0, \pm 1, ..., \pm N$ in the absence of body force and free charge can be written as

$$\frac{\partial \tau_{mxz}}{\partial x} + \frac{\partial \tau_{myz}}{\partial y} = 0, \tag{5.2.6}$$

$$\frac{\partial D_{mx}}{\partial x} + \frac{\partial D_{my}}{\partial y} = 0, \tag{5.2.7}$$

$$\frac{\partial B_{mx}}{\partial x} + \frac{\partial B_{my}}{\partial y} = 0. \tag{5.2.8}$$

With the aid of auxiliary functions η_m, χ_m, ζ_m defined by

$$\eta_m = c_{440} w_m + e_{150}\phi_m + f_{150}\psi_m, \tag{5.2.9}$$

$$\chi_m = e_{150} w_m - \epsilon_{110}\phi_m - g_{110}\psi_m, \tag{5.2.10}$$

$$\zeta_m = f_{150} w_m - g_{110}\phi_m - \mu_{110}\psi_m, \tag{5.2.11}$$

the following relations can be obtained employing equations (5.2.3)-(5.2.5) as

$$\tau_{mzk} = e^{\beta x}\frac{\partial \eta_m}{\partial k},\ D_{mk} = e^{\beta x}\frac{\partial \chi_m}{\partial k},\ B_{mk} = e^{\beta x}\frac{\partial \zeta_m}{\partial k}. \tag{5.2.12}$$

Therefore, equations (5.2.6)-(5.2.8) reduce to

$$\nabla^2\eta_m + \beta\frac{\partial\eta_m}{\partial x} = 0, \tag{5.2.13}$$

$$\nabla^2\chi_m + \beta\frac{\partial\chi_m}{\partial x} = 0, \tag{5.2.14}$$

$$\nabla^2\zeta_m + \beta\frac{\partial\zeta_m}{\partial x} = 0. \tag{5.2.15}$$

The considered problem is solved for two different crack boundary conditions which are impermeable and permeable types. The boundary conditions for the magneto-electrically impermeable cracks are given by

$$y \in [-h, h] : \tau_{mzx}(a_m, y) = D_{mx}(a_m, y) = B_{mx}(a_m, y)$$
$$= \tau_{mzx}(b_m, y) = D_{mx}(b_m, y) = B_{mx}(b_m, y) = 0, \tag{5.2.16}$$

$$x \in (a_m, b_m) : \tau_{mzy}(x, h_m) = -\tau_0,\ D_{my}(x, h_m) = -D_0,$$
$$B_{my}(x, h_m) = -B_0, \tag{5.2.17}$$

$$x \notin (a_m, b_m) : w_m(x, h_m) = \phi_m(x, h_m)$$
$$= \psi_m(x, h_m) = 0, \tag{5.2.18}$$

and for magneto-electrically permeable cracks those are given by

$$y \in [-h, h] : \tau_{mzx}(a_m, y) = D_{mx}(a_m, y) = B_{mx}(a_m, y)$$
$$= \tau_{mzx}(b_m, y) = D_{mx}(b_m, y) = B_{mx}(b_m, y) = 0, \tag{5.2.19}$$

$$x \in (a_m, b_m) : \tau_{mzy}(x, h_m) = -\tau_0, \tag{5.2.20}$$

$$x \notin (a_m, b_m) : w_m(x, h_m) = 0, \tag{5.2.21}$$

$$x \in [0, w] : \phi_m(x, h_m) = \psi_m(x, h_m) = 0, \tag{5.2.22}$$

where $h_m = mh_0$.

5.3 Solution of magneto-electrically impermeable cracks

Case I: Multiple parallel embedded cracks of equal length

Keeping in mind the geometry of the considered problem and the contributions of the articles [13, 14, 113], the complex functions Φ_{mj} $(j = 1, 2, 3)$ for magneto-electrically impermeable parallel cracks are defined as

$$\Phi_{mj} = \sum_{n=1}^{M} iA_{mjn}\sqrt{\{z-(a_m+ih_m)\}\{z-(b_m+ih_m)\}}(z-ih_m)^{n-1}, \tag{5.3.1}$$

where A_{mjn} are the real unknowns to be determined, M is the number of summation term and z is a complex number defined as $z = x+iy$ for $x, y \in \Re$. Since the problem deals with the real-valued functions, therefore the mechanical displacement, electric and magnetic potentials are given by

$$w_m = \mathrm{Re}(\Phi_{m1}), \phi_m = \mathrm{Re}(\Phi_{m2}), \psi_m = \mathrm{Re}(\Phi_{m3}). \tag{5.3.2}$$

It is clear that the first three conditions as mentioned in section 1, the complex function is already satisfied by the above choice. Only the boundary condition needs to be taken care of. Using (5.3.2), the equations (5.2.3)-(5.2.5) reduce to

$$\tau_{mzk} = c_{44}\frac{\partial \mathrm{Re}(\Phi_{m1})}{\partial k} + e_{15}\frac{\partial \mathrm{Re}(\Phi_{m2})}{\partial k} + f_{15}\frac{\partial \mathrm{Re}(\Phi_{m3})}{\partial k}, \tag{5.3.3}$$

$$D_{mk} = e_{15}\frac{\partial \mathrm{Re}(\Phi_{m1})}{\partial k} - \epsilon_{11}\frac{\partial \mathrm{Re}(\Phi_{m2})}{\partial k} - g_{11}\frac{\partial \mathrm{Re}(\Phi_{m3})}{\partial k}, \tag{5.3.4}$$

$$B_{mk} = f_{15}\frac{\partial \mathrm{Re}(\Phi_{m1})}{\partial k} - g_{11}\frac{\partial \mathrm{Re}(\Phi_{m2})}{\partial k} - \mu_{11}\frac{\partial \mathrm{Re}(\Phi_{m3})}{\partial k}. \tag{5.3.5}$$

The following expressions can be obtained with the help of Cauchy-Riemann equations as

$$\tau_{mzk} = c_{44}\mathrm{Re}\left(\frac{\partial \Phi_{m1}}{\partial k}\right) + e_{15}\mathrm{Re}\left(\frac{\partial \Phi_{m2}}{\partial k}\right) + f_{15}\mathrm{Re}\left(\frac{\partial \Phi_{m3}}{\partial k}\right), \tag{5.3.6}$$

$$D_{mk} = e_{15}\mathrm{Re}\left(\frac{\partial \Phi_{m1}}{\partial k}\right) - \epsilon_{11}\mathrm{Re}\left(\frac{\partial \Phi_{m2}}{\partial k}\right) - g_{11}\mathrm{Re}\left(\frac{\partial \Phi_{m3}}{\partial k}\right), \tag{5.3.7}$$

$$B_{mk} = f_{15}\mathrm{Re}\left(\frac{\partial \Phi_{m1}}{\partial k}\right) - g_{11}\mathrm{Re}\left(\frac{\partial \Phi_{m2}}{\partial k}\right) - \mu_{11}\mathrm{Re}\left(\frac{\partial \Phi_{m3}}{\partial k}\right). \tag{5.3.8}$$

Equation (5.3.1) gives

$$\frac{\partial \Phi_{mj}}{\partial x} = \sum_{n=1}^{M} iA_{mjn}P_{mn}, \quad \frac{\partial \Phi_{mj}}{\partial y} = \sum_{n=1}^{M} i^2 A_{mjn}P_{mn}, \tag{5.3.9}$$

where $P_{mn} = [2n(x+iy-ih_m)^n - (2n-1)(a_m+b_m)$

$\times (x+iy-ih_m)^{n-1} + 2(n-1)a_m b_m (x+iy-ih_m)^{n-2}]$

$/[2\sqrt{\{x+iy-(a_m+ih_m)\}\{x+iy-(b_m+ih_m)\}}]$.

Utilizing (5.3.9), equations (5.3.6)-(5.3.8) can be expressed as

$$\tau_{mzx} = \sum_{n=1}^{M} [c_{44}A_{m1n} + e_{15}A_{m2n} + f_{15}A_{m3n}]\,\mathrm{Re}(iP_{mn}), \tag{5.3.10}$$

$$D_{mx} = \sum_{n=1}^{M} [e_{15}A_{m1n} - \epsilon_{11}A_{m2n} - g_{11}A_{m3n}]\,\mathrm{Re}(iP_{mn}), \tag{5.3.11}$$

$$B_{mx} = \sum_{n=1}^{M} [f_{15}A_{m1n} - g_{11}A_{m2n} - \mu_{11}A_{m3n}]\,\mathrm{Re}(iP_{mn}), \tag{5.3.12}$$

$$\tau_{mzy} = \sum_{n=1}^{M} [c_{44}A_{m1n} + e_{15}A_{m2n} + f_{15}A_{m3n}]\,\mathrm{Re}(i^2P_{mn}), \tag{5.3.13}$$

$$D_{my} = \sum_{n=1}^{M} [e_{15}A_{m1n} - \epsilon_{11}A_{m2n} - g_{11}A_{m3n}]\,\mathrm{Re}(i^2P_{mn}), \tag{5.3.14}$$

$$B_{my} = \sum_{n=1}^{M} [f_{15}A_{m1n} - g_{11}A_{m2n} - \mu_{11}A_{m3n}]\,\mathrm{Re}(i^2P_{mn}). \tag{5.3.15}$$

Case II: Multiple parallel edge cracks of equal length

For this crack configuration, the complex functions Φ_{mj} $(j = 1, 2, 3)$ for magneto-electrically impermeable parallel cracks are defined as

$$\Phi_{mj} = \sum_{n=1}^{M} iA_{mjn}\sqrt{\{z - (b_m + ih_m)\}}(z - ih_m)^{n-1}. \tag{5.3.16}$$

Following a similar procedure as of Case I, the equations (5.3.6)-(5.3.8) can be expressed as

$$\tau_{mzx} = \sum_{n=1}^{M} [c_{44}A_{m1n} + e_{15}A_{m2n} + f_{15}A_{m3n}]\,\mathrm{Re}(iQ_{mn}), \tag{5.3.17}$$

$$D_{mx} = \sum_{n=1}^{M} [e_{15}A_{m1n} - \epsilon_{11}A_{m2n} - g_{11}A_{m3n}]\,\mathrm{Re}(iQ_{mn}), \tag{5.3.18}$$

$$B_{mx} = \sum_{n=1}^{M} [f_{15}A_{m1n} - g_{11}A_{m2n} - \mu_{11}A_{m3n}]\,\mathrm{Re}(iQ_{mn}), \tag{5.3.19}$$

$$\tau_{mzy} = \sum_{n=1}^{M} [c_{44}A_{m1n} + e_{15}A_{m2n} + f_{15}A_{m3n}]\,\mathrm{Re}(i^2Q_{mn}), \tag{5.3.20}$$

$$D_{my} = \sum_{n=1}^{M} [e_{15}A_{m1n} - \epsilon_{11}A_{m2n} - g_{11}A_{m3n}]\,\mathrm{Re}(i^2Q_{mn}), \tag{5.3.21}$$

$$B_{my} = \sum_{n=1}^{M} [f_{15}A_{m1n} - g_{11}A_{m2n} - \mu_{11}A_{m3n}]\,\mathrm{Re}(i^2Q_{mn}). \tag{5.3.22}$$

where $Q_{mn} = [(2n-1)(x + iy - ih_m)^{n-1} - 2(n-1)b_m(x + iy - ih_m)^{n-2}]$
$/[2\sqrt{\{x + iy - (b_m + ih_m)\}}]$.

Case III: Multiple parallel edge cracks of alternating length

In this case the expressions of complex functions, anti-plane shear stress, in-plane electric displacement, and magnetic inductions are the same as obtained for the case of multiple parallel edge cracks of equal length. The only change is in the value of b_m whose value is same for all m in Case II whereas for this case $b_{2m} < b_{2m+1}$

$(m = 0, \pm 1, ..., \pm N)$.

5.4 Solution of magneto-electrically permeable cracks

Case I: Multiple parallel embedded cracks of equal length

The complex functions Φ_{mj} $(j = 1, 2, 3)$ for magneto-electrically permeable cracks are given by

$$\Phi_{m1} = \sum_{n=1}^{M} i[A_{m1n}\sqrt{\{z-(a_m+ih_m)\}\{z-(b_m+ih_m)\}} - (pA_{m2n}+qA_{m3n})(z-ih_m)](z-ih_m)^{n-1}, \tag{5.4.1}$$

$$\Phi_{mj} = \sum_{n=1}^{M} iA_{mjn}(z-ih_m)^n, \ j = 2, 3, \tag{5.4.2}$$

where $p = e_{150}/c_{440}$ and $q = f_{150}/c_{440}$. Analogous to the impermeable case, the following expressions are obtained.

$$\frac{\partial \Phi_{m1}}{\partial x} = \sum_{n=1}^{M} i\left[A_{m1n}P_{mn} - (pA_{m2n}+qA_{m3n})R_{mn}\right], \tag{5.4.3}$$

$$\frac{\partial \Phi_{m1}}{\partial y} = \sum_{n=1}^{M} i^2\left[A_{m1n}P_{mn} - (pA_{m2n}+qA_{m3n})R_{mn}\right], \tag{5.4.4}$$

$$\frac{\partial \Phi_{mj}}{\partial x} = \sum_{n=1}^{M} iA_{mjn}R_{mn}, \quad \frac{\partial \Phi_{mj}}{\partial y} = \sum_{n=1}^{M} i^2A_{mjn}R_{mn}, \ j = 2, 3, \tag{5.4.5}$$

where $R_{mn} = n(x+iy-ih_m)^{n-1}$.

Using (5.3.18)-(5.3.20), the equations (5.3.6)-(5.3.8) for permeable type cracks can be expressed as

$$\tau_{mzx} = \sum_{n=1}^{M} c_{44}A_{m1n}\mathrm{Re}(iP_{mn}) - [c_{44}pA_{m2n} + c_{44}qA_{m3n} - e_{15}A_{m2n} - f_{15}A_{m3n}]\mathrm{Re}(iR_{mn}), \tag{5.4.6}$$

$$D_{mx} = \sum_{n=1}^{M} e_{15}A_{m1n}\mathrm{Re}(iP_{mn}) - [e_{15}pA_{m2n} + e_{15}qA_{m3n} + \epsilon_{11}A_{m2n} + g_{11}A_{m3n}]\mathrm{Re}(iR_{mn}), \tag{5.4.7}$$

$$B_{mx} = \sum_{n=1}^{M} f_{15}A_{m1n}\mathrm{Re}(iP_{mn}) - [f_{15}pA_{m2n} + f_{15}qA_{m3n} + g_{11}A_{m2n} + \mu_{11}A_{m3n}]\mathrm{Re}(iR_{mn}), \tag{5.4.8}$$

$$\tau_{mzy} = \sum_{n=1}^{M} c_{44}A_{m1n}\mathrm{Re}(i^2P_{mn}) - [c_{44}pA_{m2n} + c_{44}qA_{m3n} - e_{15}A_{m2n} - f_{15}A_{m3n}]\mathrm{Re}(i^2R_{mn}), \tag{5.4.9}$$

$$D_{my} = \sum_{n=1}^{M} e_{15}A_{m1n}\mathrm{Re}(i^2P_{mn}) - [e_{15}pA_{m2n} + e_{15}qA_{m3n} + \epsilon_{11}A_{m2n} + g_{11}A_{m3n}]\mathrm{Re}(i^2R_{mn}), \tag{5.4.10}$$

$$B_{my} = \sum_{n=1}^{M} f_{15}A_{m1n}\mathrm{Re}(i^2P_{mn}) - [f_{15}pA_{m2n} + f_{15}qA_{m3n} + g_{11}A_{m2n} + \mu_{11}A_{m3n}]\mathrm{Re}(i^2R_{mn}). \tag{5.4.11}$$

Case II: Multiple parallel edge cracks of equal length

For this case the complex functions Φ_{mj} $(j = 1, 2, 3)$ for magneto-electrically permeable cracks are given by

$$\Phi_{m1} = \sum_{n=1}^{M} i[A_{m1n}\sqrt{\{z - (b_m + ih_m)\}} - (pA_{m2n} + qA_{m3n})(z - ih_m)](z - ih_m)^{n-1}, \tag{5.4.12}$$

$$\Phi_{mj} = \sum_{n=1}^{M} iA_{mjn}(z - ih_m)^n, \ j = 2, 3. \tag{5.4.13}$$

Thus, the equations (5.3.6)-(5.3.8) reduce to

$$\tau_{mzx} = \sum_{n=1}^{M} c_{44}A_{m1n}\mathrm{Re}(iQ_{mn}) - [c_{44}pA_{m2n} + c_{44}qA_{m3n} - e_{15}A_{m2n} - f_{15}A_{m3n}]\mathrm{Re}(iR_{mn}), \tag{5.4.14}$$

$$D_{mx} = \sum_{n=1}^{M} e_{15}A_{m1n}\mathrm{Re}(iQ_{mn}) - [e_{15}pA_{m2n} + e_{15}qA_{m3n} + \epsilon_{11}A_{m2n} + g_{11}A_{m3n}]\mathrm{Re}(iR_{mn}), \tag{5.4.15}$$

$$B_{mx} = \sum_{n=1}^{M} f_{15}A_{m1n}\mathrm{Re}(iQ_{mn}) - [f_{15}pA_{m2n} + f_{15}qA_{m3n} + g_{11}A_{m2n} + \mu_{11}A_{m3n}]\mathrm{Re}(iR_{mn}), \tag{5.4.16}$$

$$\tau_{mzy} = \sum_{n=1}^{M} c_{44}A_{m1n}\mathrm{Re}(i^2Q_{mn}) - [c_{44}pA_{m2n} + c_{44}qA_{m3n} - e_{15}A_{m2n} - f_{15}A_{m3n}]\mathrm{Re}(i^2R_{mn}), \tag{5.4.17}$$

$$D_{my} = \sum_{n=1}^{M} e_{15}A_{m1n}\mathrm{Re}(i^2Q_{mn}) - [e_{15}pA_{m2n} + e_{15}qA_{m3n} + \epsilon_{11}A_{m2n} + g_{11}A_{m3n}]\mathrm{Re}(i^2R_{mn}), \tag{5.4.18}$$

$$B_{my} = \sum_{n=1}^{M} f_{15}A_{m1n}\mathrm{Re}(i^2Q_{mn}) - [f_{15}pA_{m2n} + f_{15}qA_{m3n} + g_{11}A_{m2n} + \mu_{11}A_{m3n}]\mathrm{Re}(i^2R_{mn}). \tag{5.4.19}$$

Case III: Multiple parallel edge cracks of alternating length

Again, in this case, the expressions of complex functions, anti-plane shear stress, in-plane electric displacement, and magnetic inductions are the same as of Case II with only a change in the value of b_m.

5.5 Driving force parameters

The stress intensity factors at the crack tips are determined by

$$K_{III}^{a_m,(m)} = \lim_{x\to a_m} \sqrt{2\pi(a_m - x)}\ \tau_{mzy}(x, h_m), \tag{5.5.1}$$

$$K_{III}^{b_m,(m)} = \lim_{x\to b_m} \sqrt{2\pi(x - b_m)}\ \tau_{mzy}(x, h_m). \tag{5.5.2}$$

In terms of A_{mjn}, the crack tip stress intensity factors for multiple parallel embedded cracks of equal length for magneto-electrically impermeable cracks are given by

$$K_{III}^{a_m,(m)} = e^{\beta a_m}\sqrt{\frac{\pi(b_m - a_m)}{2}}\ \sum_{n=1}^{M} a_m^{n-1}\left(c_{440}A_{m1n} + e_{150}A_{m2n} + f_{150}A_{m3n}\right), \tag{5.5.3}$$

$$K_{III}^{b_m,(m)} = -e^{\beta b_m}\sqrt{\frac{\pi(b_m - a_m)}{2}}\ \sum_{n=1}^{M} b_m^{n-1}\left(c_{440}A_{m1n} + e_{150}A_{m2n} + f_{150}A_{m3n}\right), \tag{5.5.4}$$

and for magneto-electrically permeable cracks those are given by

$$K_{III}^{a_m,(m)} = e^{\beta a_m}\sqrt{\frac{\pi(b_m - a_m)}{2}}\ \sum_{n=1}^{M} a_m^{n-1} c_{440}A_{m1n}, \tag{5.5.5}$$

$$K_{III}^{b_m,(m)} = -e^{\beta b_m}\sqrt{\frac{\pi(b_m - a_m)}{2}}\ \sum_{n=1}^{M} b_m^{n-1} c_{440}A_{m1n}. \tag{5.5.6}$$

The crack tip stress intensity factors for multiple parallel edge cracks of equal as well as alternating lengths for magneto-electrically impermeable cracks are determined by

$$K_{III}^{b_m,(m)} = -e^{\beta b_m}\sqrt{\frac{\pi}{2}}\ \sum_{n=1}^{M} b_m^{n-1}\left(c_{440}A_{m1n} + e_{150}A_{m2n} + f_{150}A_{m3n}\right), \tag{5.5.7}$$

and for magneto-electrically permeable cracks those are determined by

$$K_{III}^{b_m,(m)} = -e^{\beta b_m}\sqrt{\frac{\pi}{2}}\sum_{n=1}^{M} b_m^{n-1} c_{440} A_{m1n}. \tag{5.5.8}$$

The stress magnification factors at the crack tips [102, 103] are determined by

$$M_{III}^{a_m,(m)} = \frac{K_{III}^{a_m,(m)}}{K_{III}^{a_m,(m)*}},\ M_{III}^{b_m,(m)} = \frac{K_{III}^{b_m,(m)}}{K_{III}^{b_m,(m)*}}, \tag{5.5.9}$$

where $K_{III}^{a_m,(m)*}$ and $K_{III}^{b_m,(m)*}$ are the crack tip SIFs of the m^{th} crack in the absence of remaining cracks for the concerned case.

5.6 Results and discussion

The boundary collocation method is used to solve the equations (5.3.9)-(5.3.14), (5.3.17)-(5.3.22), (5.4.2)-(5.4.3). It is sufficient to take into account only the positive portion of the y-axis due to geometric symmetry. For numerical computation, some points on the external boundaries of the plane and crack surfaces are chosen. Here A_{mjn}'s are the unknowns to be determined. If the number of equations is equal to the total number of unknowns then the unknowns can be determined by using the concept of matrix inversion [113]. Usually, to improve the accuracy more points are to be taken so that the number of equations is greater than the total number of unknowns, and the least square method is employed to obtain the coefficients [85]. The parameters are assumed to be $c_{440} = 54$ GPA, $e_{150} = 7.8$ C/m^2, $\epsilon_{110} = 3.64 \times 10^{-9}$ C^2 /Nm^2, $f_{150} = 175$ N /Am, $\mu_{110} = -1.97 \times 10^{-4}$ Ns^2 /C^2, $g_{110} = 0.8 \times 10^{-11}$ Ns /(VC), $\tau_0 = 4.2 \times 10^6$ N /m^2 [120]. While determining A_{mjn}'s, M is chosen in such a way that three decimal digit accurate values of crack tip SMFs are

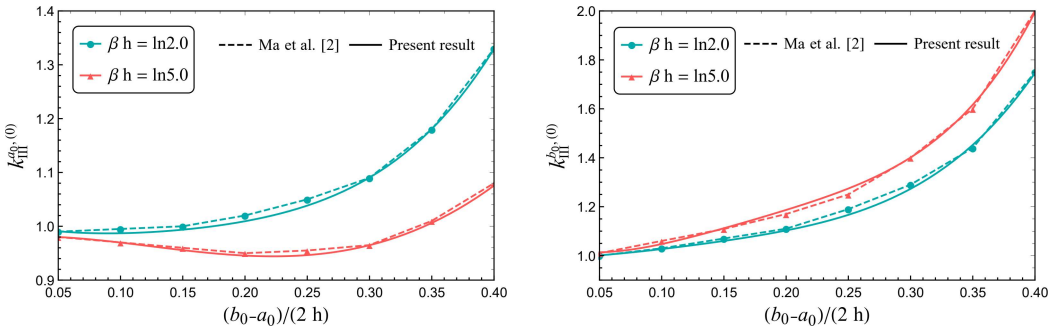

(a) **(b)**

Figure 5.6.1: Comparison between obtained and existing results [71] of normalized SIFs at the crack tip (a) a_0 and (b) b_0 as a function of normalized crack length $(b_0 - a_0)/(2h)$ for distinct values of normalized functionally graded parameter βh for a single embedded crack in a functionally graded magneto-electro-elastic strip.

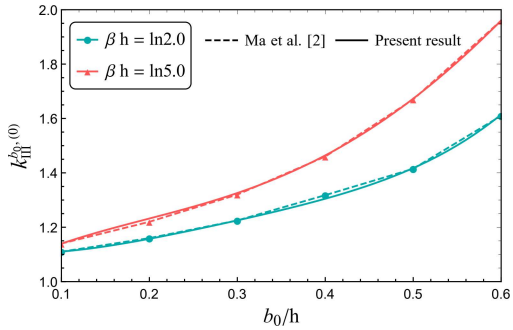

Figure 5.6.2: Comparison between obtained and existing results [71] of normalized SIFs at the crack tip b_0 as a function of normalized crack tip b/h for distinct values of normalized functionally graded parameter βh for a single edge crack in a functionally graded magneto-electro-elastic strip.

acquired. For Case I, $a_m/h = 0.2$, $b_m/h = 0.4$; Case II, $b_m/h = 0.4$ and Case III, $b_{2m}/h = b_{01} = 0.2$, $b_{2m+1}/h = b_{02} = 0.4$ have been taken.

5.6.1 Validation

This section of the chapter presents a validation to compare the obtained results with the results provided in [71]. The integral transform and dislocation density functions

have been used in [71] to tackle the problem of a magneto-electrically impermeable or permeable embedded and edge crack perpendicular to the boundary of a functionally graded magneto-electro-elastic strip.

By taking into consideration a single crack, $N = 0$ in the direction of x-axis, and for $h >> b_0$, the current problem is reduced to [71]. For $c_{440} = 44$ GPA, $e_{150} = 5.8$ C/m^2, $\epsilon_{110} = 6.46 \times 10^{-9}$ C^2 /Nm^2, $f_{150} = 275$ N /Am, $\mu_{110} = -2.97 \times 10^{-4}$ Ns^2 /C^2, $g_{110} = 0.5 \times 10^{-11}$ Ns /(VC), $\tau_0 = 4.2 \times 10^6$ N /m^2, $\lambda_d = 0$ and $\lambda_b = 0$ [120], the findings of both the studies are compared for both embedded and edge crack configurations. It can be seen from Figures 5.6.1 and 5.6.2 that the results obtained by our proposed method are in good agreement with the existing results provided in [71], when the normalized SIFs at the cracks' tips a_0 and b_0 are denoted by $k_{III}^{a_0,(0)}$ and $k_{III}^{b_0,(0)}$, respectively and normalizing factor of SIFs for embedded and edge crack is taken into account as $\tau_0\sqrt{\pi(b_0 - a_0)/2}$ and $\tau_0\sqrt{\pi b_0}$, respectively.

5.6.2 Significance of functionally graded parameter

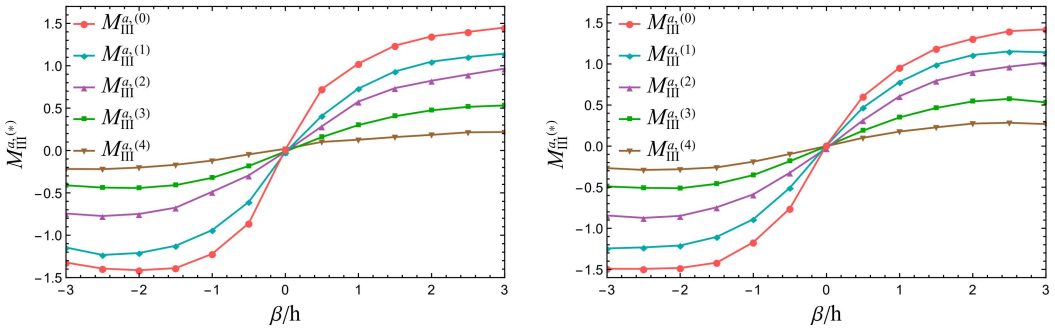

Figure 5.6.3: Variations in SMFs at the crack tip a as a function of normalized functionally graded parameter β/h under magneto-electrically (a) impermeable condition and (b) permeable condition for Case I.

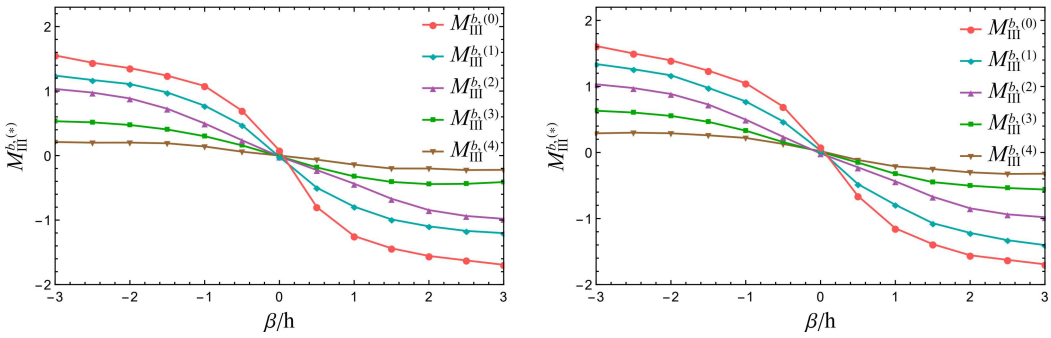

Figure 5.6.4: Variations in SMFs at the crack tip b as a function of normalized functionally graded parameter β/h under magneto-electrically (a) impermeable condition and (b) permeable condition for Case I.

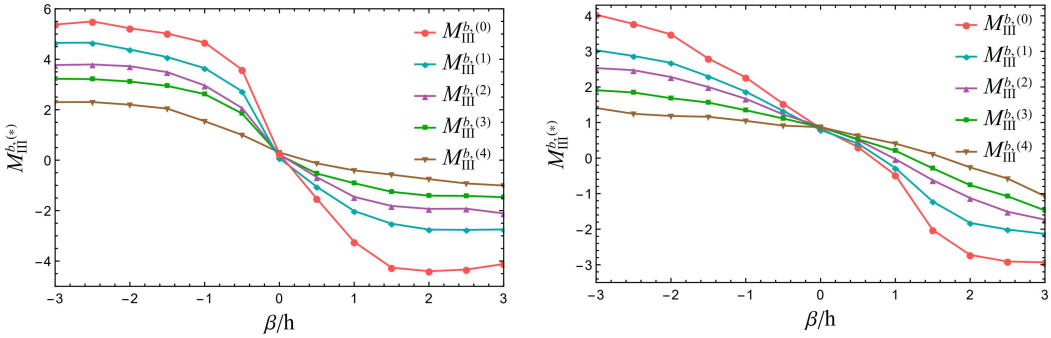

Figure 5.6.5: Variations in SMFs at the crack tip b as a function of normalized functionally graded parameter β/h under magneto-electrically (a) impermeable condition and (b) permeable condition for Case II.

Figures 5.6.3, 5.6.4, 5.6.5, and 5.6.6 illustrate how functionally graded parameters affect crack tip SMFs in both magneto-electrically impermeable and permeable conditions. As β/h increases, SMF increases at the left crack tips in Case I, as shown in Figure 5.6.3. In contrast, it decreases at the right crack tips with the increasing value of β/h for all three cases as demonstrated from Figures 5.6.4, 5.6.5 and 5.6.6. This shows that the likelihood of crack amplification increases at the left crack tip as the value of the functionally graded parameter increases, whereas the likelihood of crack shielding increases at the right crack tip.

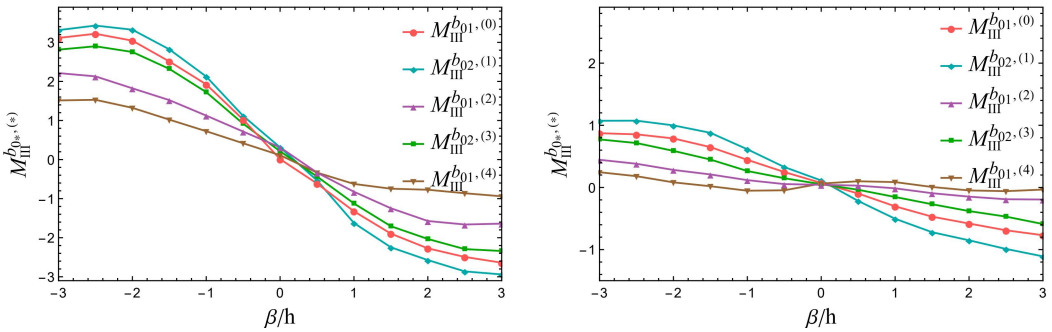

Figure 5.6.6: Variations in SMFs at the crack tip b_0 as a function of normalized functionally graded parameter β/h under magneto-electrically (a) impermeable condition and (b) permeable condition for Case III.

Upon examination of the results, it is evident that for the negative value of β/h the possibility of crack shielding is high for inner cracks in comparison to the outer ones whereas for the positive value of β/h the possibility of crack amplification is high for outer cracks in comparison to the inner ones at the left crack tips under Case I. On the other hand at the right crack tip for the negative value of β/h the possibility of crack amplification is high for inner cracks while for the positive value of β/h the possibility of crack shielding is high for outer cracks for the Cases I and II. In Case III, it is noted that for negative values of the functionally graded parameter, the crack amplification phenomenon is high for longer cracks, while for positive values, the shielding phenomenon is high for shorter cracks.

Additionally, under magneto-electrically impermeable and permeable conditions, the magnitude of the SMFs at the crack tips varies in all cases. This indicates that the crack arrest tendency differs between magneto-electrically impermeable and permeable conditions.

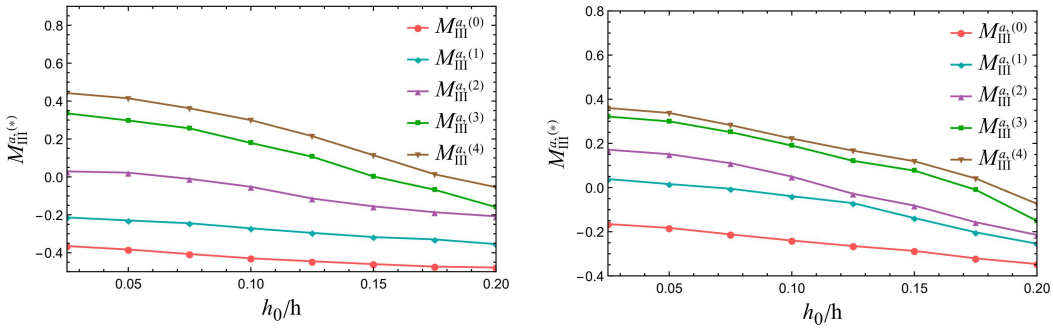

Figure 5.6.7: Plots of SMFs at the crack tip a as a function of normalized crack spacing h_0/h under magneto-electrically (a) impermeable condition and (b) permeable condition for Case I.

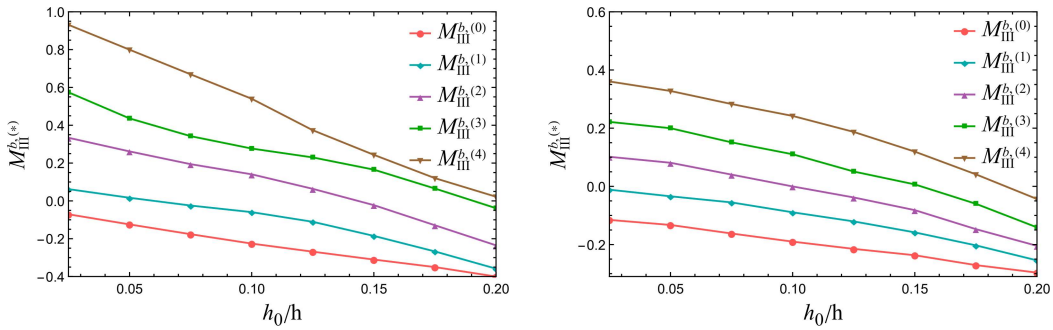

Figure 5.6.8: Plots of SMFs at the crack tip b as a function of normalized crack spacing h_0/h under magneto-electrically (a) impermeable condition and (b) permeable condition for Case I.

5.6.3 Significance of crack spacing

Figures 5.6.7, 5.6.8, 5.6.9, and 5.6.10 illustrate how crack spacing affects the likelihood of crack arrest. For both the impermeable and permeable type cracks, it is observed that as the spacing between the cracks increases the crack tip SMFs are started to decrease which arises the possibility of cracks' arrest. In Cases I and III, only shielding behavior is noticed while both shielding and amplification behavior is noticed in Case II.

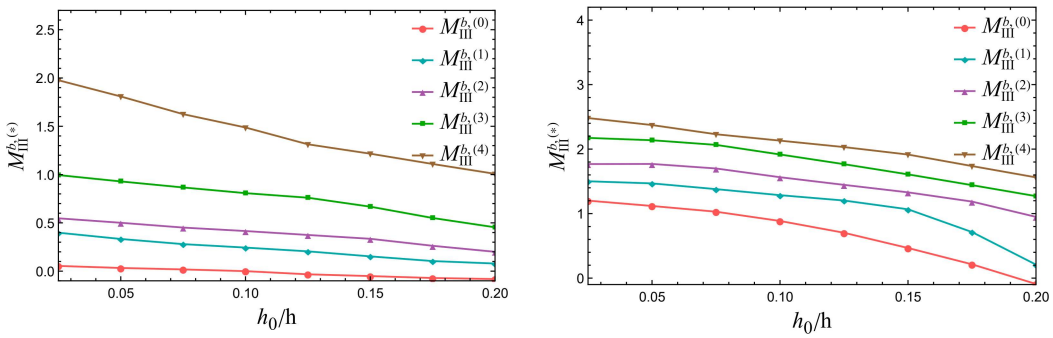

Figure 5.6.9: Plots SMFs at the crack tip b as a function of normalized crack spacing h_0/h under magneto-electrically (a) impermeable condition and (b) permeable condition for Case II.

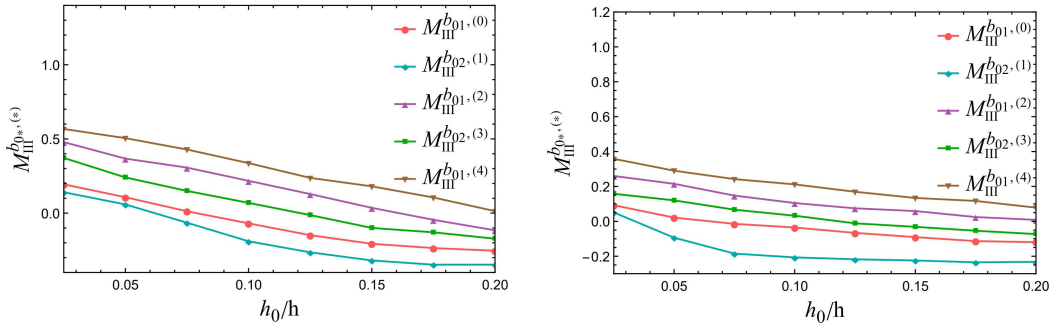

Figure 5.6.10: Plots of SMFs at the crack tip b_0 as a function of normalized crack spacing h_0/h under magneto-electrically (a) impermeable condition and (b) permeable condition for Case III.

Additionally, in Cases I and II, under both magneto-electrically impermeable and permeable conditions, the magnitude of the crack tip SMFs for outer cracks is greater than that for inner cracks. For Case III, it can be shown that the shorter cracks have an elevated magnitude of crack tip SMFs than the longer ones. The magneto-electrically impermeable and permeable conditions significantly affect the tendency of cracks to arrest, as shown in Figures 5.6.7, 5.6.8, 5.6.9, and 5.6.10.

5.6.4 Significance of electric and magnetic loads

The shielding and amplification behavior of permeable type cracks are unaffected by the electric and magnetic loads. However, the effects of both loads are depicted in Figures 5.6.11, 5.6.12, 5.6.13 and 5.6.14 for the impermeable type cracks. As per the figure keeping the magnetic load fixed if the electric load increases then the cracks started to arrest at both crack tips. Whereas, for fixed electric load and increasing magnetic load, the cracks are started to propagate. In other words, electric loads resist the propagation of cracks whereas magnetic load enhances the propagation of cracks.

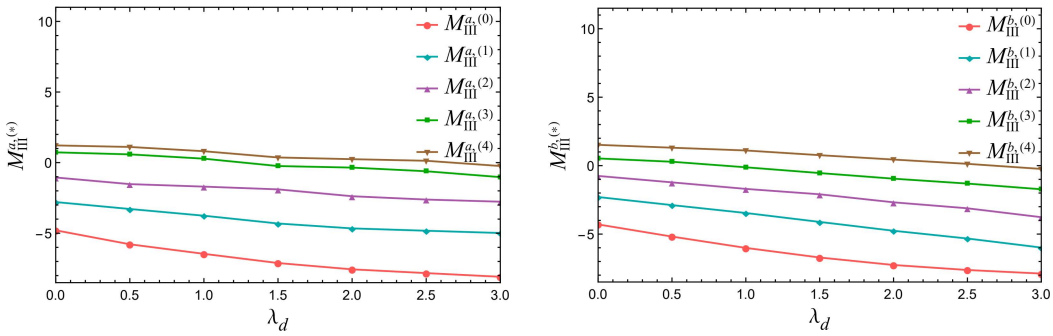

Figure 5.6.11: Influence of electric load λ_d on SMFs for Case I at the crack tip (a) a and (b) b.

5.7 Concluding remarks

The possibility of multiple parallel magneto-electrically impermeable and permeable cracks being arrested for three different configurations of cracks is examined in this chapter under the impact of gradient parameter, the distance between the cracks, and electric and magnetic loadings. The semi-analytical forms of SIFs and SMFs are obtained for all three crack configuration cases by expressing the displacement

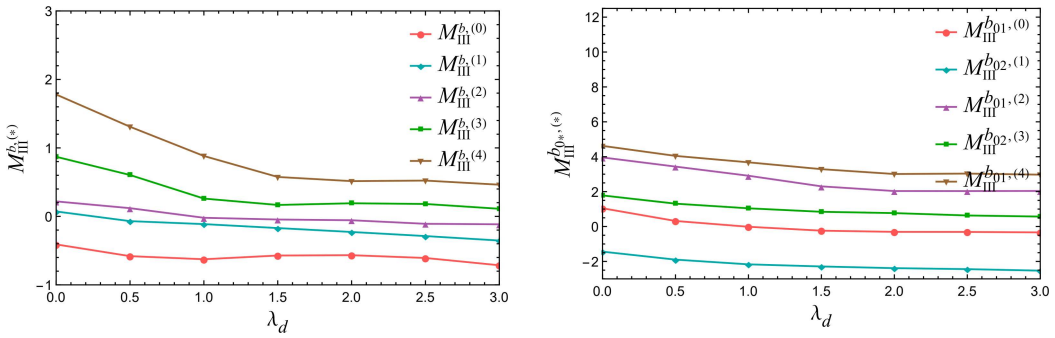

(a) **(b)**

Figure 5.6.12: Influence of electric load λ_d on SMFs at the crack tip b for (a) Case II and (b) Case III.

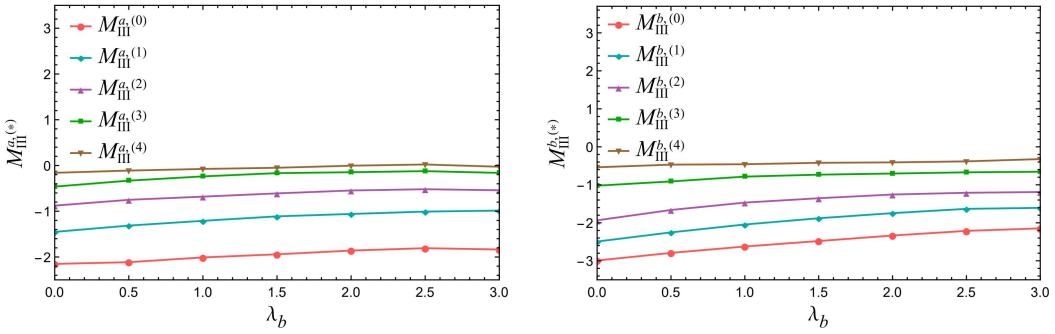

(a) **(b)**

Figure 5.6.13: Influence of magnetic load λ_b on SMFs for Case I at the crack tip (a) a and (b) b.

and potential functions in terms of power series and applying boundary collocation and least square methods. The followings are the findings of the current study:

1. The semi-analytical expressions of SIFs that aid in calculating the crack tip SMFs for the cases under consideration.

2. In all three crack configuration scenarios, the changes in the values of the functionally graded parameter have a considerable impact on the likelihood of crack arrest.

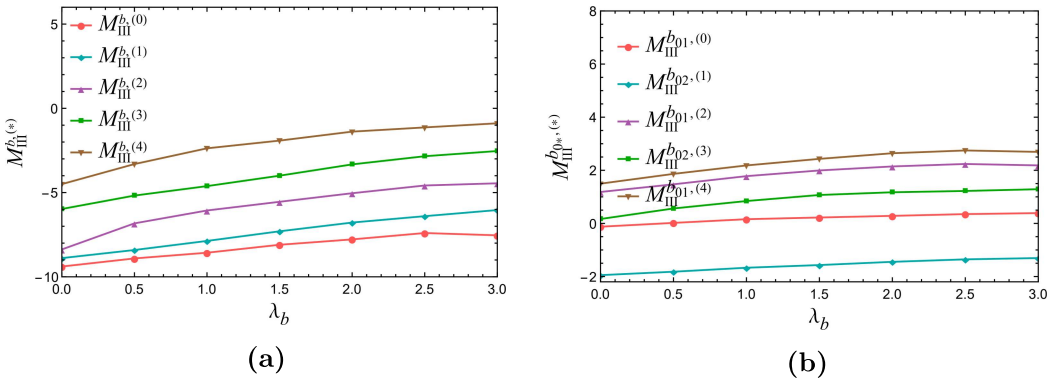

Figure 5.6.14: Influence of magnetic load λ_b on SMFs at the crack tip b for (a) Case II and (b) Case III.

3. The graphical displays of SMFs as a function of crack distance show that the interaction of cracks plays a non-negligible role in the shielding and amplifying nature of parallel cracks of different configurations. The crack arrest is less likely to occur as the distance between the cracks started to reduce.

4. With an increase in the electric load and a decrease in the magnetic load, the cracks have a greater tendency to be arrested.

5. The distinction between parallel cracks, which are magneto-electrically impermeable and permeable for different cases are graphically illustrated using SMFs.

6. The innermost cracks have the smallest magnitude and the outermost cracks have the largest magnitude when there are multiple parallel embedded and edge cracks of equal length. The shorter edge cracks have a magnitude greater than the longer ones when there are multiple parallel edge cracks of varying lengths.

****